Swirling Flow in Thrust Nozzles

H. Doyle Thompson* and Joe D. Hoffmann*
Purdue University, West Lafayette, Indiana

This paper investigates the effects of adding swirl to a dump combustor-nozzle propulsion system. The results of cold-flow testing are summarized and compared to a numerical analysis of the nozzle flowfield. The cold-flow testing included thrust, mass flow rate, and pressure measurements for two different conical nozzles in combination with four swirlers, one of which was a blank. Five-port probe measurements were made across the nozzle entrance. The measurements were used to determine the stagnation pressure and swirl distributions and to provide initial conditions for a nozzle analysis program. The measured results show that swirl has a strong effect on the stagnation pressure distribution. The largest losses occur near the swirl axis. Swirl also significantly reduces the system discharge coefficient. In contrast, the effect of swirl on the nozzle stream thrust efficiency was small, but measurable. Swirl reduced the nozzle stream thrust efficiency by about 0.5% for the highest swirl tested. Computed nozzle flowfields that do not account for the stagnation pressure distribution in the swirling flow can produce highly distorted and unrealistic results. Comparison of measured and computed results (which use measured stagnation pressure and swirl distributions) shows reasonable agreement.

Nomenclature

A,B,C = constants in curve fit equations
A = area
A_e = nozzle exit area (20.029 in.^{2}, 12,922 mm^2)
A_f = fixture cross-sectional area (38.705 in.^{2}, 24,971 mm^2)
A^* = nozzle throat area (11.782 in.^{2}, 7601.3 mm^2)
C_D = discharge coefficient
C_{D_m} = measured discharge coefficient
CA.4 = constant-angle swirler with swirl number $S = 0.4$
CA.5 = constant-angle swirler with swirl number $S = 0.5$
F_i = ideal stream thrust (zero ambient pressure)
F_m = measure thrust
F_s = stream thrust
FV.4 = free-vortex swirler with swirl number $S = 0.4$
K_1 = dimensional constant defined by Eq. (9) (16.7922 in.^{2} = 10,833.7 mm^2)
K_2 = slope of F_s vs P_t data, Eq. (12)
M_e = ideal exit Mach number ($M_e = 2.0088$)
$\dot{m}_i$ = ideal mass flow rate, Eq. (3)
$\dot{m}_m$ = measured mass flow rate
P_o = measured nozzle inlet stagnation pressure from five-port probe
P_t = measured system stagnation pressure upstream of swirlers
p_a = atmospheric pressure
p_b = ambient (base) pressure
R = radial coordinate of flow passage, or gas constant
R_t = radius of nozzle throat (1.9365 in., 49.187 mm)
r = radial coordinate
S = swirl number defined by Eq. (1)
SPR = system pressure ratio (P_t/p_b)
T_t = measured system stagnation temperature
V_r, V_θ, V_z = velocity components in the r-, θ-, and z-coordinate directions
Y_1, Y_2 = inner and outer radii of an axisymmetric flow passage
z = axial coordinate
α = swirl angle, i.e., the angle between the velocity vector and its projection onto the r-z plane
γ = specific heat ratio (1.4 for air)
Γ = specific heat ratio function defined by Eq. (4) (0.810185 for air)
η_s = stream thrust efficiency
θ = radial flow angle, i.e., the angle between the z direction and the projection of the velocity vector onto the r-z plane
ρ = density

Received March 7, 1988; revision received Jan. 18, 1989.

*Professor, School of Mechanical Engineering. Associate Fellow AIAA.

Introduction

RECENT studies indicate that the introduction of swirl ahead of the combustor in axisymmetric dump combustors can have a beneficial effect on the combustion process. Buckley et al.[1] found that swirl both reduced the reattachment length of the combustor flowfield (thereby reducing the overall combustor length needed for good performance) and greatly reduced destructive, very-low-frequency instabilities. They did not, however, determine the effect of swirl on the propulsive system performance. This is an important question, since differences of 1 or 2% are critical in ramjet and scramjet operation.

Recently several attempts have been made to determine the effects of swirl on nozzle performance using well-developed computer codes.[2-4] These methods are basically sound but they require realistic initial conditions across the nozzle entrance. The required variables are usually the stagnation temperature and pressure T_t and P_t, either the radial velocity V_r or the radial flow angle θ, and either the tangential swirl velocity V_θ or the swirl angle α. For nonswirling flows, a simplistic uniform flow assumption has led to reasonably good results. For swirling flows, however, the assumption of a uniform stagnation pressure is unrealistic and produces unrealistic results. For example, Fig. 1 presents computed Mach number contours for a flow with swirl at the nozzle entrance, with uniform stagnation pressure and temperature. The uniform stagnation pressure assumption results in supersonic contour lines that run upstream parallel to the nozzle axis, a ridiculous result.

Experimental measurements that can provide the needed initial value information are lacking. Scharrer and Lilley[5] made five-hole pitot probe measurements of the effects of

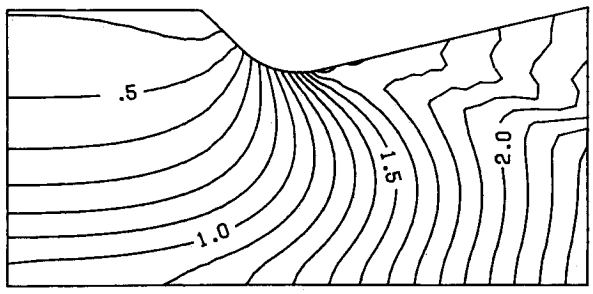

Fig. 1 Computed Mach number contours for uniform stagnation pressure for the long conic nozzle with the CA.5 swirler.

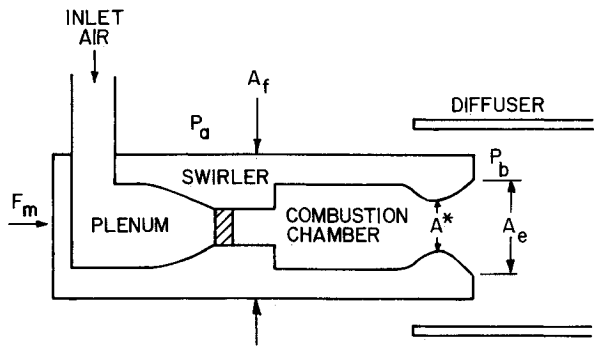

Fig. 2 Flow system.

swirl in simulated dump combustors followed by a nozzle. They observed a significant interaction between the swirling flowfield in the simulated combustor and the nozzle flowfield. Their major objective, however, was the measurement of the confined turbulent flow in the simulated combustor, not the nozzle flowfield. Consequently, their nozzles were simply used as downstream blockage components.

Reference 6 presents a summary and analysis of a series of tests that were conducted specifically to determine the effects of swirl on the performance of several thrust nozzles. The objective of the present paper is to organize and summarize the data from Ref. 6, and to compare the experimental results with the results from a recently developed analytical method. High-quality measurements were made that can be used as benchmark data for the development of analytical models to predict engine, swirler, combustor, and nozzle performance. The tests were cold-flow experiments in a flow geometry that is representative of a dump combustor for ramjets. The flow system is illustrated in Fig. 2. Metered air at near-constant stagnation temperature and pressure was diffused and swirl introduced by a set of swirl vanes. The flow then expanded through a sudden-expansion section, passed through a simulated constant-diameter combustor section, and then through the thrust nozzle.

Measurements of thrust and pressures were made so that discharge coefficients and stream thrust efficiencies could be determined for the system. In addition, five-port probe measurements were made at selected radial positions across the nozzle entrance. The five-port probe data were used to evaluate cold-flow stagnation pressure losses in the swirler and sudden-expansion section. The measured values were also used as initial data for a nozzle analysis program. Experimental and computed nozzle performance parameters are compared.

Test Procedures and Measurements

The test setup and details of the measurement techniques are described in Ref. 6. This section discusses the measurements that were made, their accuracy, consistency, and overall reliability.

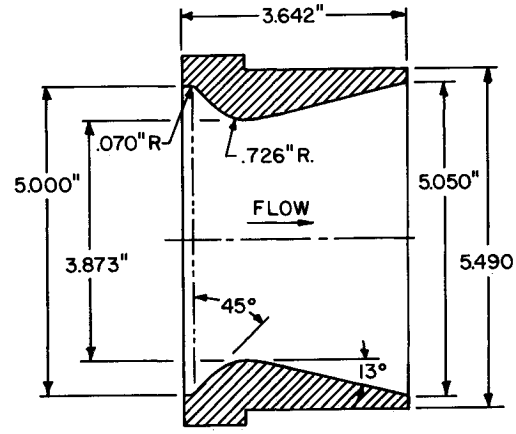

Fig. 3 Geometry of the long conic nozzle.

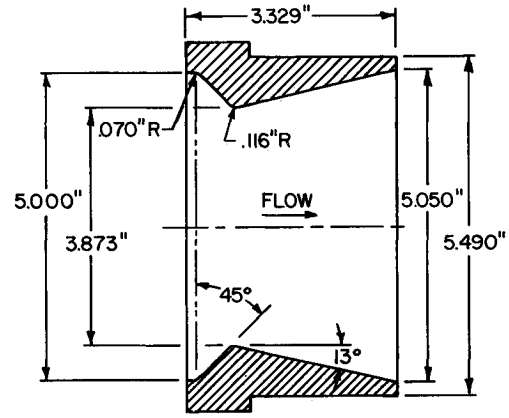

Fig. 4 Geometry of the short conic nozzle.

Figure 2 illustrates the flow system for the tests. The entire assembly is mounted on a pendulum-type support that can be rotated 180 deg (i.e., from right-flowing to left-flowing) so that two measurements can be taken. Normal procedure is to average the right- and left-flowing results to eliminate biases arising from any misalignment of the incoming flow. The support fixture allows for the independent interchange of swirlers and nozzles. Test results were obtained for three swirlers and a blank swirler insert in combination with two conical nozzles. Two of the swirlers were designed to produce near-constant swirl angles at their exit with swirl numbers of 0.4 and 0.5. They are hereafter designated as the CA.4 and CA.5 swirlers. The swirl number S is a global measure of the swirl in the flowfield. It is defined as

$$S = \frac{\int_{Y_1}^{Y_2} (rV_\theta)\, \rho V_z r\, dr}{Y_2 \int_{Y_1}^{Y_2} V_z\, \rho V_z r\, dr} \tag{1}$$

The third swirler, designated as the FV.4 swirler, was designed to produce a free-vortex swirl distribution with a swirl number of 0.4. The two conical nozzles have the same throat and exit areas. They are designated as the long conic nozzle and the short conic nozzle, as they differ primarily in the length of the subsonic sections. The details of the nozzle geometries are illustrated in Figs. 3 and 4.

Measurements were made for each of the eight swirler-nozzle combinations over a range of system pressure ratios (SPR). Eight or nine atmospheric exhaust tests were made at SPRs between 2 and 6. For each atmospheric exhaust test, both right- and left-flowing measurements were made and averaged. The atmospheric exhaust tests were all repeated to check for consistency. The repeated test results were compared to the original test results, and all were found to be consistent to within the overall experimental measurement tolerances, which were of the order of 0.1–0.2%.

To extend the SPR values, a diffuser (ejector) system was used. The diffuser lowered the effective back pressure for the system so that SPRs from about 3 to 25 were possible. The diffuser runs consisted of 15–16 tests at SPR values over that range. For the diffuser tests, it was not practical to rotate the test assembly, so only right-flowing results were obtained.

In addition to the atmospheric and diffuser tests, a series of tests were made in which the stagnation pressure, static pressure, and swirl angle just ahead of the nozzle were measured using a five-port probe. Measurements were made at r/R values of 0, ± 0.4, and ± 0.8.

For every data point and every run, the mass flow rate $\dot{m}_m$, stagnation temperature T_t, stagnation pressure upstream of the swirlers P_t, and the ambient pressure p_a were measured. Static pressure measurements were also made at eight locations around the base of the nozzle, at five locations in the diffuser (when it was used), and at five locations around the housing just upstream of the nozzle entrance. Mass flow rates were measured ahead of the support fixture by a pair of parallel, calibrated ASME venturi meters. The mass flow rate measurements are estimated to be accurate and consistent to within $\pm 0.1\%$.

Stagnation temperature measurements were made in the upstream plenum and as part of the venturi mass flow rate measurement. The stagnation temperature varied somewhat from day to day and even a few degrees during a long run on the same day. The measurements appear to be repeatable and to give correct differences between runs. It is hard to evaluate the absolute accuracy of the stagnation temperature measurements under run conditions, but there is no indication that temperature measurement error is a problem in these tests.

Stagnation pressures were varied between 30 and 75 psia and were measured in the plenum chamber upstream of the swirler. The stagnation pressure measurements appear to be consistent between runs. There is an unexplained inconsistency between the plenum stagnation pressure and the five-port probe stagnation pressure. This inconsistency is discussed in the Directional Probe Data and Results section. There is no reason to suspect that inaccuracies in the ambient pressure or the static pressure measurements are large enough to cause significant errors in the results.

Axial thrust measurements were made for each of the atmospheric exhaust and diffuser runs. The thrust measurements were repeatable, but for the atmospheric exhaust runs, the measured values differed by 5–10 lbf between the left- and right-flowing orientations. The thrust measurements for the right-flowing orientation were consistently below those for the left-flowing orientation. The difference increased with an increase in the stagnation pressure.

System Performance Measurements

From the measured mass flow rates, pressures, temperatures, and thrust values, the measured system discharge coefficient C_{D_m} and the measured system stream thrust efficiency η_s for each of the eight swirler-nozzle combinations were determined. The system discharge coefficient is the ratio of the measured to the ideal mass flow rates:

$$C_{D_m} = \dot{m}_m/\dot{m}_i \tag{2}$$

The ideal mass flow rate is computed assuming one-dimensional isentropic choked flow through the minimum area (throat) A^*. One form of the $\dot{m}_i$ equation is[7]

$$\dot{m}_i = P_t \Gamma A^*/(\gamma R T_t)^{1/2} \tag{3}$$

where

$$\Gamma = \gamma\,[2/(\gamma+1)]^{(\gamma+1)/2(\gamma-1)} \tag{4}$$

Thus,

$$C_{D_m} = \frac{\dot{m}_m\, T_t^{1/2}}{P_t}\left[\frac{(\gamma R)^{1/2}}{\Gamma A^*}\right] \tag{5}$$

Measurements of $\dot{m}_m$, T_t, and P_t were made for each of the eight swirler-nozzle combinations over a range of SPRs. The discharge coefficients were independent of SPR as expected, and were extremely consistent. The measured values for the eight swirler-nozzle combinations are tabulated in Table 1. The estimated accuracy is ± 0.001.

The discharge coefficients are for the system (i.e., swirler, sudden-expansion section, and nozzle). Therefore, the values are much lower than one would expect for the nozzle alone. The difficulty with determining a discharge coefficient for the nozzle is, of course, the lack of well-defined reference conditions for the nozzle.

There are several measures of thrust efficiency. The stream thrust efficiency is used here because it is a measure of the system internal performance and is independent of the ambient conditions. The stream thrust efficiency is the ratio of the total internal stream thrust produced by the system F_s, to the ideal stream thrust at zero ambient pressure F_i:

$$\eta_s = F_s/F_i \tag{6}$$

To eliminate the effect of the discharge coefficient, the measured mass flow rate is used to calculate the ideal stream thrust. The ideal stream thrust is computed from the equation

$$F_i = \frac{\dot{m}_m\,(T_t R/\gamma)^{1/2}(1+\gamma M_e^2)}{M_e\left(1+\dfrac{\gamma-1}{2}M_e^2\right)^{1/2}} \tag{7}$$

Each of the nozzles tested had the same throat and exit areas and had an area ratio of 1.700, which corresponds to an ideal $M_e = 2.0088$.

Substituting $(C_{D_m}\,\dot{m}_i)$ for $\dot{m}_m$ in Eq. (7), where $\dot{m}_i$ is given by Eq. (3), yields

$$F_i = K_1\, C_{D_m}\, P_t \tag{8}$$

where K_1 is the dimensional constant

$$K_1 = \frac{\Gamma A^*(1+\gamma M_e^2)}{\gamma M_e\left(1+\dfrac{\gamma-1}{2}M_e^2\right)^{1/2}} \tag{9}$$

Table 1 Summary of measured system discharge coefficients and stream thrust efficiencies

Nozzle	Swirler	$C_{D_m}(\pm 0.001)$	K_2	η_s
Long conic	Blank	0.943	15.658	0.9888
	CA.4	0.809	13.400	0.9864
	CA.5	0.756	12.550	0.9840
	FV.4	0.762	12.622	0.9864
Short conic	Blank	0.916	15.219	0.9894
	CA.4	0.800	13.235	0.9852
	CA.5	0.753	12.431	0.9838
	FV.4	0.751	12.449	0.9872

The stagnation temperature T_t cancels, so that K_1 is a function of only the specific heat ratio and nozzle geometry.

The measured internal thrust F_s is determined from the measured thrust plus corrections for ambient pressure operation. The inlet air is introduced perpendicular to the measured thrust direction. The mechanism and methods for eliminating errors are described in Ref. 8. The total internal stream thrust F_s is the integral of the axial momentum flux plus the pressure thrust across the nozzle exit. Using a control volume approach, the axial momentum equation corresponding to Fig. 2 can be reduced to

$$F_s = F_m + p_b A_e + A_f(p_a - p_b) \tag{10}$$

For atmospheric exhaust tests, $p_a = p_b$, and F_s is determined by simply adding $p_b A_e$ to F_m. Thus,

$$F_s = F_m + p_b A_e \quad \text{(atmospheric exhaust)} \tag{11}$$

When the measured stream thrust efficiencies are compared for different SPRs, the efficiencies are high for the lowest SPR values and are even greater than 100% for some of the atmospheric tests. This behavior results from flow separation in the nozzle. From examination of the data for all eight systems, it appears that separation occurs below SPRs of about 3.5. Therefore, data for SPRs < 3.5 are omitted from the system efficiency computations.

For all eight systems, the stream thrust efficiencies for the diffuser runs are consistently below the atmospheric exhaust runs by about 1%. That difference is illustrated in Fig. 5, where least-squares linear fits to the two sets of data for the long conic nozzle and the CA.4 swirler (without the SPR < 3.5 results) are presented. It appears that there is consistent bias and/or a tare force associated with the diffuser operation that is not present in the atmospheric exhaust tests. This bias is partially explained by the difference in testing procedure. For the atmospheric exhaust tests, the measured thrust for the right-flowing system is consistently below that of the left-flowing system by as much as 1%. Differences of 5–10 lbf were almost always recorded at the higher pressures. When the diffuser was used, only right-flowing measurements were made, which accounts for a large portion of the differences in the test results. The atmospheric exhaust tests are considered to be the more accurate. From the data, it was not possible to identify other measurement bias.

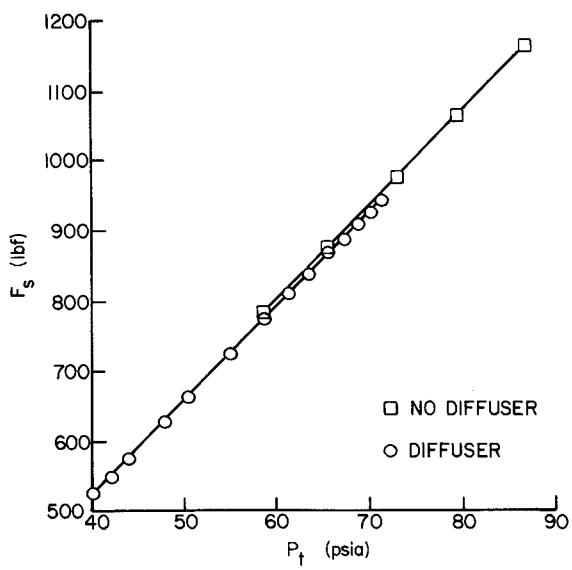

Fig. 5 Stream thrust vs plenum stagnation pressure for the long conic nozzle and CA.4 swirler.

Least-squares linear curve fits through the origin were made of the P_t vs F_s data for the atmospheric exhaust runs for SPRs > 3.5 and for each of the eight swirler-nozzle combinations. Each curve fit is of the form

$$F_s = K_2 P_t \tag{12}$$

The measured stream thrust efficiency for the system is

$$\eta_s = \frac{F_s}{F_i} = \frac{K_2}{K_1 C_{D_m}} \tag{13}$$

where F_i from Eq. (8) is used. Table 1 presents a tabulation of the measured K_2 values and the system stream thrust efficiency results.

It is apparent from the results presented in Table 1 that the principal effect of adding swirl is to change the system discharge coefficient. Stagnation pressure losses in the swirler and the sudden-expansion section reduce the system discharge coefficient, but because the measured mass flow rate is used in the ideal stream thrust definition, those losses cancel in the stream thrust efficiency calculation. The stream thrust efficiency is the efficiency of the thrust nozzle, for which the primary loss is the flow divergence loss.

The stream thrust efficiency measurements are estimated to be accurate to about ±0.2%. Swirl degrades the stream thrust efficiency by about 0.3–0.5%. It is quite possible that if the nozzles were designed for swirling flow, some portion of that loss could be recovered.

Directional Probe Data and Results

A five-port probe was used to make flowfield measurements downstream of the swirler and sudden-expansion section at 0.5 in. (12.7 mm) upstream of the nozzle entrance and at five radial locations across the diameter of the entrance section. The radial locations were at r/R values of ±0.8, ±0.4, and 0.0. For each measurement, the probe was rotated to null the two static pressure ports aligned with the swirl. The swirl angle was read from the attached protractor. At that orientation, the central port measured the stagnation pressure. The measurements at the two nonnulled ports were used with the calibration curve to determine the radial velocity component. The measurements were corrected using the calibration curves for the probe, and values for swirl angle, stagnation pressure, static pressure, axial velocity, radial velocity, and swirl velocity were computed.

Eight runs were made in all. Two runs each (at a pressure ratio of 3.0 and 4.0, respectively) were made with each of the three swirlers and with the blank swirler insert. The nozzle used to maintain choked flow for the eight runs was neither the long nor short conic nozzle, but was a conic nozzle with an airfoil-shaped bar across the center. The throat area of the bar nozzle was the same as that of the long and short conic nozzles, and the contraction geometry was similar to the long conic nozzle. The bar across the nozzle was in the transonic-supersonic region. The five-port probe measurements were made at radial locations perpendicular to the bar. It is tacitly assumed that the measured values of P_o and α are dependent only on the swirler and sudden-expansion section geometry and are not affected by the presence of the bar or by the difference in the geometry of the subsonic convergence section of the nozzle.

The stagnation pressure profiles were measured by setting the flow conditions and traversing the probe to different r/R locations in sequence. The plenum stagnation pressure P_t and temperature T_t drifted slightly between each point measurement. The P_t values varied as much as 1.0 psi between point sets. Measured P_t values were used to normalize the stagnation pressure measurements. Comparison of the measurements at plus and minus values of r/R showed axial symmetry. Stagna-

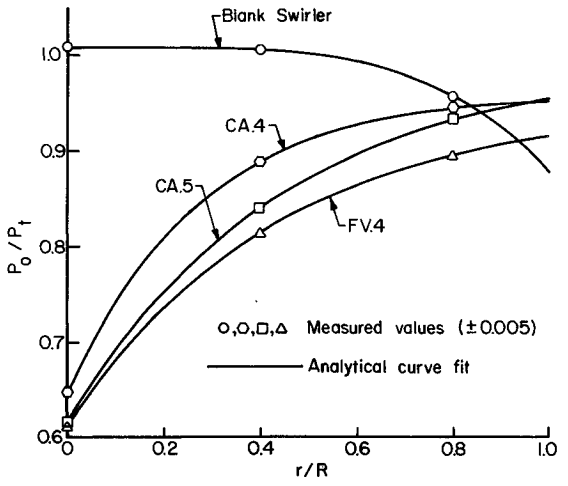

Fig. 6 Stagnation pressure profiles at the nozzle entrance.

tion pressure ratios were averaged for the plus and minus measurements and for both pressure ratios at each radial location. Individual measurements were all within ±0.5% of the average for the CA.5 and FV.5 swirlers and were within ±0.2% for the blank and CA.4 swirlers. The average values are plotted in Fig. 6.

The stagnation pressure profile data were fit to appropriate curves. For the blank swirler, the stagnation pressure is fairly constant across the central portion of the flowfield and drops off near the wall. This is in accord with the expected behavior. That profile is fit to the curve

$$P_o/P_t = A - B(r/R)^C \tag{14}$$

where $A = 1.0080$, $B = 0.1323$, and $C = 4.3055$. Figure 6 presents the curve fit and the experimental measurements. The curve fit gives a value of $P_o/P_t = 0.8757$ at the wall and an area-averaged value of $(P_o/P_t)_{aa} = 0.9661$.

The one disturbing feature of the data is that, for the blank swirler, the measured P_o values at $r/R = 0.0$ and 0.4 are larger than the corresponding P_t measurements. Although the difference is less than 1.0%, it is disturbing, since it represents a physical impossibility. A recheck of the data has failed to locate the cause of the discrepancy. It is not known whether this represents an instrumentation discrepancy that would bias all the results, or is a discrepancy peculiar to the blank swirler insert.

The stagnation pressure data for swirlers CA.4, CA.5, and FV.4 are also presented in Fig. 6. When swirl is present, stagnation pressure losses occur near the axis. The stagnation pressure profiles for all three swirlers were fit to an exponential curve of the form

$$P_o/P_t = A + Be^{C(r/R)} \tag{15}$$

where A, B, and C are computed to fit the measured average values at $r/R = 0.0$, 0.4, and 0.8. The curves in Fig. 6 represent the following curve-fit equations:

$$P_o/P_t = 0.9596 - 0.3122e^{-3.6926(r/R)} \quad \text{(CA.4 swirler)} \tag{16}$$

$$P_o/P_t = 1.0018 - 0.3856e^{-2.1631(r/R)} \quad \text{(CA.5 swirler)} \tag{17}$$

$$P_o/P_t = 0.9520 - 0.3405e^{-2.2558(r/R)} \quad \text{(FV.4 swirler)} \tag{18}$$

The measured swirl angle profiles were fit to the following equations:

$$\alpha = 43.323\,[1 - e^{-4.8188(r/R)}] \quad \text{(CA.4 swirler)} \tag{19}$$

$$\alpha = 50.641\,[1 - e^{-4.2124(r/R)}] \quad \text{(CA.5 swirler)} \tag{20}$$

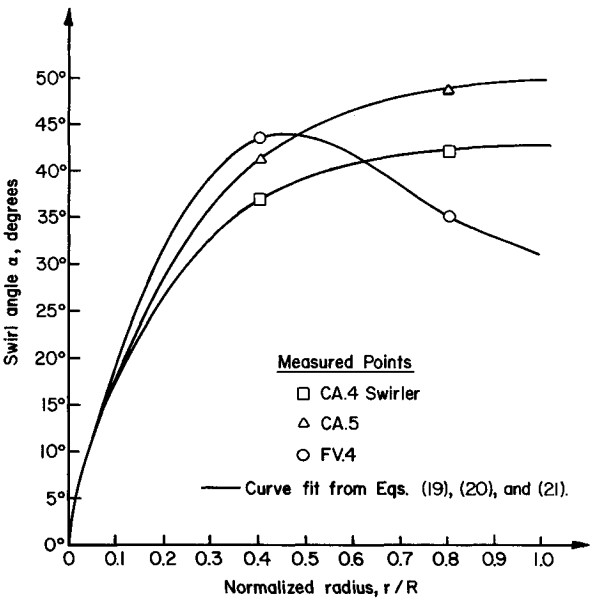

Fig. 7 Swirl angle profiles at the nozzle entrance.

$$\alpha = 224.85(r/R) - 354.53(r/R)^2 + 160.67(r/R)^3$$

(FV.4 swirler) (21)

In Eqs. (19-21), α is in degrees. To arrive at Eqs. (19) and (20), an exponential curve was assumed, and the curve was forced to go through $\alpha = 0$ at $r/R = 0.0$. The measured values at $r/R = 0.4$ and 0.8 were used to determine the constants in the equations. For the free-vortex swirler, the exponential curve produced unrealistic values at small r/R values, and a quadratic fit gave unrealistic values at large r/R values. Equation (21) is a cubic that was fit to the data at $r/R = 0.4$ and 0.8 (assuming $\alpha = 0$ at $r/R = 0.0$) and to the judiciously chosen value of $\alpha = 31$ deg at $r/R = 1.0$.

Figure 7 presents the measured swirl angle data and the swirl angle profiles from Eqs. (19-21). From the data it is apparent that the swirl angle distribution is significantly altered by the sudden-expansion section. A check of the free-vortex swirler shows rV_θ values of 31.5 and 52.3 ft/s at r/R positions of 0.4 and 0.8, respectively. Thus, if the free-vortex swirler produced a free-vortex profile (rV_θ = constant) at the swirler exit, that profile is considerably distorted at the nozzle entrance.

Analytical Method

The finite-difference code developed by Marcum and Hoffman[9] was used to calculate the nozzle flowfield. That program solves unsteady, three-dimensional, inviscid flowfields in superelliptical nozzles with centerbodies. An option exists for calculating unsteady axisymmetric inviscid flowfields in nozzles having circular cross sections. The gasdynamic model is based on the following assumptions: 1) unsteady three-dimensional flow, 2) inviscid nonconducting fluid with no body forces, and 3) a simple system in thermodynamic equilibrium. In the present analysis, the fluid was assumed to be a thermally and calorically perfect gas.

The analysis is based on the unsteady Euler equations. The finite-difference algorithm uses MacCormack's explicit finite-difference method[10] at interior points and Kentzer's method[11] at all boundary points. A Cartesian grid is superimposed at the centerline to eliminate the indeterminancy arising there when cylindrical coordinates are used. The method is capable of predicting both unsteady and steady flowfields. Steady-state flowfields are obtained by marching in time until the solution converges to a steady state.

The initial value data at the nozzle entrance were specified from the five-port probe data. The stagnation pressure distri-

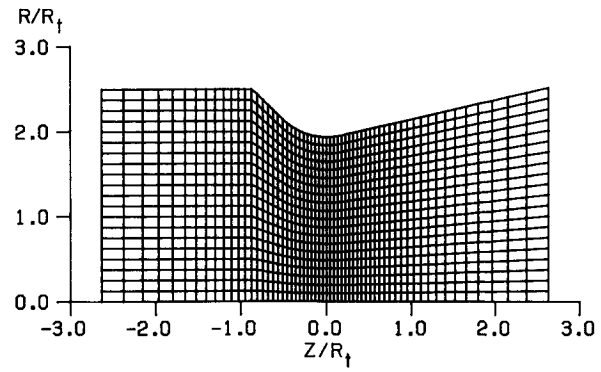

Fig. 8 Finite-difference grid for the long conic nozzle.

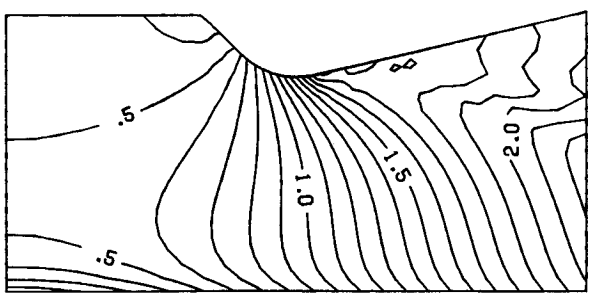

Fig. 9 Computed Mach number contours for the long conic nozzle with the CA.4 swirler.

butions presented in Fig. 6 were specified. The stagnation temperature was assumed to be uniform over the nozzle entrance, and the swirl angle distributions presented in Fig. 7 were specified. The radial velocity component was assumed to be zero at the nozzle entrance. The initial Mach-number distribution in the nozzle at time zero was specified based on one-dimensional isentropic steady flow. The Mach-number distribution across the nozzle inlet at subsequent times is part of the transient solution. Steady-state convergence is assumed when the maximum percent change in the flow properties between successive time steps is less than 0.001.

Figure 8 presents the finite-difference grid for the long conic nozzle. There are 21 equally spaced points in the radial direction and 61 points in the axial direction. The axial grid spacing is controlled by a transformation that packs the grid in the transonic region. The grid spacing technique is described in detail in Ref. 9. For the eight swirler-nozzle combinations, the flowfields were marched to steady-state, which required from 1000–1500 time steps for the long conic nozzle and about 4000 time steps for the short conic nozzle. The short conic nozzle flowfields were rerun with a 41×121 grid to about 5000 time steps. The converged solutions were essentially identical to the results for the 21×61 grid.

Figure 9 presents computed Mach number contours for the long conic nozzle with the CA.4 swirler. Comparison with Fig. 1 shows the dramatic effect of inlet stagnation pressure distribution on the Mach number profiles.

The discharge coefficient is determined by integrating the steady-state mass flow rate across the minimum area section of the nozzle. The stream thrust efficiency is determined by integrating the static pressure forces on the nozzle wall and the momentum flux and static pressure forces across the nozzle throat. The reference mass flow rate is determined from Eq. (3), where the stagnation pressure is the area-averaged value. Area-averaged values are determined by integrating the pressure profiles in Fig. 6. The reference stagnation pressure P_t for the calculation was 100 psia. The computed mass flow rate was used to determine the reference axial thrust.

Results and Summary

Table 2 presents the measured and computed nozzle discharge coefficients and stream thrust efficiencies. The measured nozzle discharge coefficients are based on the measured area-averaged stagnation pressure ahead of the nozzle. That is, the system discharge coefficients in Table 1 have been divided by the ratio $(P_o/P_t)_{aa}$ to obtain nozzle discharge coefficients. Since the computed values of the discharge coefficient are based on the same area-averaged stagnation pressure, the measured and computed results are directly comparable.

The following observations were made:

1) Swirl has a strong effect on the stagnation pressure distribution downstream of the swirler and sudden-expansion section. The losses in stagnation pressure are greatest near the axis. The magnitude and distribution of the stagnation pressure losses are a function of the geometry of the swirler and sudden-expansion section. These losses in the swirler and combustor reduce the discharge coefficient and the nozzle thrust efficiency.

2) Swirl has the following effects on the thrust nozzle performance, as determined from the experimental results: a) Swirl significantly reduces the discharge coefficient of a nozzle. The magnitude of the reduction depends on both the swirl intensity and the swirl profile entering the nozzle. b) Swirl decreases the stream thrust efficiency by a small amount. The loss increases with swirl intensity, as would be expected. The stream thrust efficiency degradation was only 0.5% for the highest swirl intensity tested. c) Accounting for only divergence losses in a 13-deg conical nozzle gives a stream thrust efficiency of $\eta_s = 0.9812$, which compares very closely with the measured value for the blank swirler.

3) Computed nozzle flowfields that do not account for the stagnation pressure distribution at the nozzle entrance can be highly distorted and unrealistic.

4) Comparsion of the measured and computed values for the long conic nozzle indicates the following: a) The computed discharge coefficients are consistently about 2–2.5% greater than the measured values. The trends match. The difference is due, at least partially, to neglecting the effects of viscosity in

Table 2 Summary of nozzle performance results

			Discharge coefficient, C_D		Stream thrust efficiency, η_s	
Nozzle	Swirler	$(P_o/P_t)_{aa}$	Measured	Calculated	Measured	Calculated
Long conic	Blank	0.9661	0.9761	0.9958	0.9888	0.9874
	CA.4	0.9160	0.8832	0.9017	0.9864	0.9841
	CA.5	0.8969	0.8468	0.8724	0.9840	0.9826
	FV.4	0.8638	0.8826	0.9071	0.9864	0.9857
Short conic	Blank	0.9661	0.9481	0.9725	0.9894	0.9951
	CA.4	0.9160	0.8734	0.8698	0.9852	0.9897
	CA.5	0.8969	0.8390	0.8441	0.9838	0.9888
	FV.4	0.8638	0.8698	0.8670	0.9872	0.9916

the numerical computations. b) The measured and calculated stream thrust efficiencies agree within experimental error. The effect of discharge coefficient is cancelled in the stream thrust determination. The very close agreement indicates that numerical efficiency computations with accurate initial conditions and relatively gentle flow geometry are accurate enough not only to evaluate design differences but also to provide absolute performance efficiencies.

5) Comparsion of the measured and computed values for the short conic nozzle indicates the following: a) The measured and computed discharge coefficients are within about 0.5% of each other. The fact that they agree more closely than the values for the long conic nozzle is probably fortuitous. The steeper subsonic entrance flow and small radius of curvature at the throat result in less accurate numerical calculations. In addition, it is not clear that the measured stagnation pressure distribution, swirl angle distribution, and radial flow distribution for the short conic nozzle are adequately represented by the measured values with the bar nozzle. This would influence both the measured and computed results. b) The calculated stream thrust efficiencies are about 0.5% higher than the measured values. The trends match so that the computed solutions can be used to evaluate design differences.

6) The measured discharge coefficients are essentially independent of system pressure ratio. The stream thrust efficiencies are likewise nearly pressure ratio-independent as long as separation does not occur in the nozzle.

Acknowledgments

The experimental measurements were conducted by McDonnell Douglas Astronautics Company, St. Louis (MDAC-STL). The experimental testing and data analysis were sponsored by AFAPL/POPR, Wright Patterson AFB.

References

[1]Buckley, P. L., Craig, R. R., Davis, D. L., and Schwartzkopf, K. G., "The Design and Combustion Performance of Practical Swirlers for Integral Rocket/Ramjets," *AIAA Journal*, Vol. 21, May 1983, pp. 733-740.

[2]Kornblum, B. T., Thompson, H. D., and Hoffman, J. D., "An Analytical Investigation of Swirl in Annular Propulsive Nozzles," *Journal of Propulsion and Power*, Vol. 2, March-April 1986, pp. 155-160.

[3]Hoffman, J. D., Thompson, H. D., and Marcum, D. L., "An Analytical Study of Swirl Effects in Annular Propulsive Nozzles," *Journal of Propulsion and Power*, Vol. 3, Sept.-Oct. 1987, pp. 465-466.

[4]Dutton, J. C., "Time-Dependent Calculation of Swirling Nozzle Flow," 1983 USAF-SCEEE Summer Faculty Research Program, Air Force Office of Scientific Research, Final Rept., Aug. 1983.

[5]Scharrer, G. L., and Lilley, D. G., "Five-Hole Pitot Probe Measurements of Swirl, Confinement, and Nozzle Effects on Confined Turbulent Flow," AIAA Paper 84-1605, June 1984.

[6]Thompson, H. D., and Hoffman, J. D., "Ramjet Nozzle Data Analysis," Rept. PHD-86-2, March 1987.

[7]Zucrow, M. J., and Hoffman, J. D., *Gas Dynamics*, Vol. 1, Wiley, New York, 1975, Chapt. 4.

[8]Conley, R. R., "High Pressure Ratio Testing with a Nozzle Driven Ejector," AIAA Paper 84-1488, June 1984.

[9]Marcum, D. L. and Hoffman, J. D., "Calculation of Three-Dimensional Inviscid Flowfields in Propulsive Nozzles with Centerbodies," *Journal of Propulsion and Power*, Vol. 4, March-April 1988, pp. 172-179.

[10]MacCormack, R. W., "The Effect of Viscosity in Hypervelocity Impact Cratering," AIAA Paper 69-354, April 1969.

[11]Kentzer, C. P., "Discretization of Boundary Conditions on Moving Discontinuities," Second International Conference on Numerical Method in Fluid Dynamics, Berkeley, CA, Sept. 1970. Published in *Lecture Notes in Physics*, Vol. 8, Springer-Verlag, New York, pp. 108-113.